www.czasopisma.pan.pl PAN POLSKA AKADEMIA NAUK www.journals.pan.pl

Arch. Min. Sci. **66** (2021), 1, 43-56

Electronic version (in color) of this paper is available: http://mining.archives.pl

DOI 10.24425/ams.2021.136691

WEIYU ZHENG[1,2*]

EXPERIMENTAL AND THEORETICAL STUDY ON THE DYNAMIC EJECTION PROCESS OF A ROCK BURST UNDER A STATIC LOAD

As the duration of a rock burst is very short and the roadway is seriously damaged after the disaster, it is difficult to observe its characteristics. In order to obtain the dynamic characteristics of a rock burst, a modified uniaxial compression experiment, combined with a high-speed camera system is carried out and the process of a rock burst caused by a static load is simulated. Some significant results are obtained: 1) The velocity of ejected particles is between 2 m/s and 4 m/s. 2) The ratio of elastic energy to plastic energy is about five. 3) The duration from integrity to failure is between 20 ms and 40 ms. Furthermore, by analyzing the stress field in the sample with a numerical method and crack propagation model, the following conclusions can be made: 1) The kinetic energy of the ejected particles comes from the elastic energy released by itself. 2) The ratio of kinetic energy to elastic energy is between 6% and 15%. This can help understand the source and transfer of energy in a rock burst quantitatively.

Keywords: rock burst; high-speed camera; kinetic energy; stress field; crack propagation

1. Introduction

A rock burst is one of the rock dynamic disasters. In the past three years, many rock burst cases occurred in China, resulting in many deaths and destroyed properties. On October 20, 2018, Shandong Energy Group Longyun mine suffered a rock burst, killing 21 people. On June 9, 2019, Jilin Coal Industry Corporation Longjiabao Mine suffered a rock burst, killing 9 people. On August 2, 2019, Kailuan (Group) Co., Ltd. Tangshan Mine suffered a rock burst, killing 7 people. Fig. 1 shows the state of a roadway before and after a rock burst. As a special type of

[1] CHINA UNIVERSITY OF MINING & TECHNOLOGY (BEIJING), SCHOOL OF ENERGY AND MINING ENGINEERING
[2] STATE KEY LABORATORY OF COAL MINING AND CLEAN UTILIZATION, CHINA

* Corresponding author: weiyuz@foxmail.com

(before) (after)

Fig. 1. Rock burst case

rock failure, the mechanism of a rock burst is a very important issue in rock mechanics. Previously, there has been a lot of experimental and theoretical research on this topic.

Some researchers have carried out mechanical experiments on the study of a rock burst. True tri-axial unloading experiment is a very effective method in studying the dynamic process of a rock burst. With this method, F. Ren et al. [1] found that a shearing concentration occurs at the bottom of the ejection position and a tensile zone is located in the fracture plane of the ejection block. G.S. Su et al. [2] found a "quiescent period" at the eve of a rock burst. F. Gong et al. [3] believed that the process of a rock burst can be divided into four periods: the calm period, the small grain ejection & spalling damage period, the slab buckling & fragment ejection period and the violent ejection period. Some researchers used uniaxial cyclic loading and unloading experiments to predict the possibility of a rock burst occurrence and evaluate the stability of rock during mining [4-6]. M. Cai believed that rock bursting has a typical brittle failure characteristic and that brittle failure mainly appears as a brittle fracture under low stress by using acoustic emission (AE) technology [7]. Some researchers designed a large scale field test with dynamic rock bolts subjected to a rock burst loading. It can be used to apply a dynamic load to a larger panel of surface support and to the four bolts, which is essential for studying the dynamic mechanical properties of rocks [8].

On the other hand, some researchers conducted a lot of theoretical studies. Simon [9] concluded that the main factor leading to the destruction of rock is not only the magnitude of the stress but also the ratio of the strength of coal and rock. Cook [10] stated that the stiffness of the mine structure is greater than the stiffness of the mine load system, which is a necessary condition for a rock burst. Calder and Madsen [11] believed that a rock burst is likely to occur when the energy released is more than the energy consumed. Some researchers believed that the burst propensity of rock is a necessary condition for a rock burst [12-14].

Whether experimentally or theoretically, different researchers mainly focus on two points. Firstly, the elastoplastic mechanics is believed that rock burst occurs when the rock meets certain mechanical boundary conditions. Secondly, the types of rock fracture are studied, which are divided into tensile failure and shear failure. Rock burst is a dynamic phenomenon, which is shown by the rapid ejection of fragments. This process was studied by the method of unloading experiments or dynamic loading experiments. In this paper, a simulation experiment of a rock burst caused by a static load is carried out. The process of a rock burst is recorded by a high-speed camera. The mechanism of a rock burst is comprehensively discussed with the load-deformation curve and the crack propagation mechanics.

2. Characteristics and classification of rock burst

Rock burst is a type of disaster caused by the sudden and violent release of a large amount of elastic strain energy accumulated in the surrounding rock. Excavation is the external cause of rock burst, which changes the original stress balance. After rebalanced, the stress of the surrounding rock is concentrated. It can be released from the free surface in the roadways, which causes rock burst disasters in brittle rock. Different types of rock burst are caused by different stress states. The unexcavated underground rock is under triaxial balanced stress. Because of the excavation, the stresses of the surrounding rock on both sides of the roadway change into a uniaxial compression state.

Rock bursts are often accompanied by seismic events, which can be used to classify rock bursts [15]. In approximate ascending order of energy magnitude, the main source mechanisms are considered. A simplified basis for differentiation of these categories in terms of essential nature and seismic magnitude is given in table 1 [16].

TABLE 1

Rock burst categories

Seismic Event	Postulated Source Mechanism	First Motion from Seismic Records	Richter Magnitude M_L
Strain-bursting	Superficial spalling with violent ejection of fragments	Usually undetected; could be implosive	–0,2 to 0
Buckling	Outward expulsion of pre-existing larger slabs parallel to opening	implosive	0 to 1,5
Face crush	Violent expulsion of rock from tunnel face	implosive	1.0 to 2.5
Shear rupture	Violent propagation of shear fracture through intact rock mass	Double-couple shear	2.0 to 3.5
Fault-slip	Violent renewed movement on existing fault	Double-couple shear	2.5 to 5.0

The essential nature of the first three source mechanisms is different from those of the last two. The significance of this observation is that for the first three mechanisms, the source and damage locations are probably coincident and the rock involved in the source is also involved in the damage. For example, rock bursting occurs right at the surface of the opening, and it is strongly influenced by the local shape and stress concentration of that surface. Unstable failures represented by buckling and face crushing are also affected by the openings in their immediate vicinity. In contrast, the last two mechanisms represent a shear failure on a plane, and the extent of this shear failure zone could be hundreds of meters. Such conditions are likely to occur only in association with large-scale mining operations.

The locations of the rock bursts and seismic sources must be different. Generally speaking, these two locations in strain-induced rock burst cases are basically the same. On the contrary, shear failure often occurs away from the location of the rock burst and acts on the free surface of the roadway through the form of seismic waves [17]. Some scholars have conducted in-depth researches on the shear failure of rock and rock mass [18]. This paper analyses the mine pillar rock burst, which is the main type of strain-induced rock burst. Rock bursts occur very quickly, usually lasting from a few seconds to a few minutes. In addition, rock bursts have no obvious

sign before they happen and after the disaster, the roadways are seriously damaged, as shown in Fig. 1. Therefore, the rock burst simulation experiment can be an effective method to obtain the characteristics of the process of a rock burst.

3. Experimental study

When rock bursts occur, the compressed rock is destroyed into small pieces, causing some particles to be ejected rapidly through obtaining kinetic energy. This phenomenon can occur even under static load. It is a unique characteristic that is different from other types of rock failures. Hence this experiment has been designed to study this process.

3.1. Experiment plan

The samples taken from a mine affected by rock burst are processed into ∅50 mm × 100 mm cylinder. The following are the mechanical parameters measured before the experiment:

- Density: 1474.87kg/m^3;
- Compressive strength: 33.08MPa;
- Elastic modulus: 2474.80 MPa;
- Poisson's ratio: 0.321;
- Internal friction angle: 46.21°;
- Cohesion: 8.10MPa;
- Tensile strength: 1.031MPa.

The experiment layout is shown in Fig. 2.

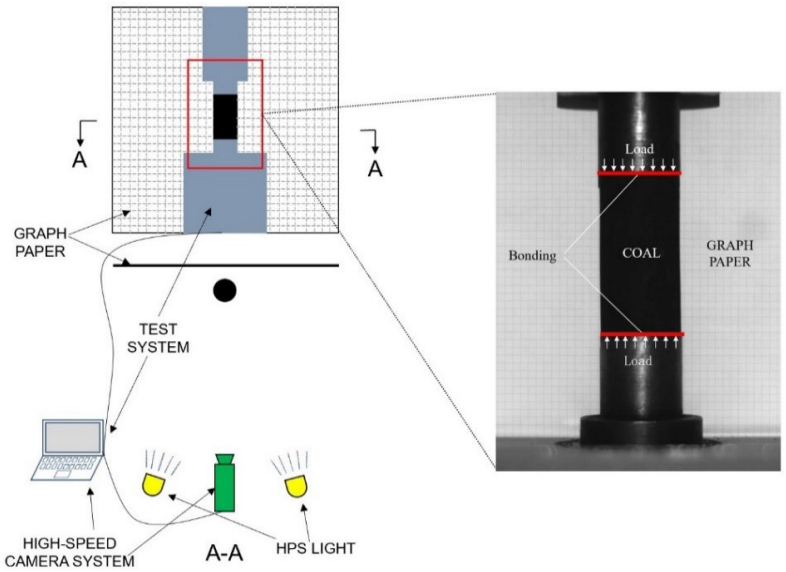

Fig. 2. Experiment layout

The graph paper should be fixed on the rigid testing machine, followed by adjusting the location of the high-speed camera before the experiment. The camera exposure time is set to 2 ms, and the interval is set to 3 ms. The high-pressure sodium (HPS) on both sides of the camera should be turned on. The graph paper should be as close as possible to the sample, and the high-speed camera should be as far away from the sample as possible. In order to simulate the stress state of the mine pillar, both ends of the sample are fixed on the test machine with glue, which is equivalent to applying a radial fixed boundary condition. The reason is as follows: regardless of the room-pillar mining method or long-wall mining method, both ends of the mine pillar are together with the surrounding rock.

During the experiment, the state of the sample should be observed carefully. Once a particle ejection occurs, the system should be unloaded immediately. The experiment is carried out according to the following steps:

1) Measuring the height, diameter and mass of the sample;
2) Applying glue to ends of the sample and fixing it on the testing machine;
3) Applying a preload of 1000 N to the sample;
4) Loading at an increasing rate of 500 N/s, monitoring the stress and deformation, and recording the entire test process with a high-speed camera;
5) Unloading the sample after the ejection occurs;
6) Removing the sample and processing experimental data.

3.2. Results

Five uniaxial compressions tests are carried out (Test 1-Test 5) in this experiment. The images taken by the high-speed camera are shown in Fig. 3.

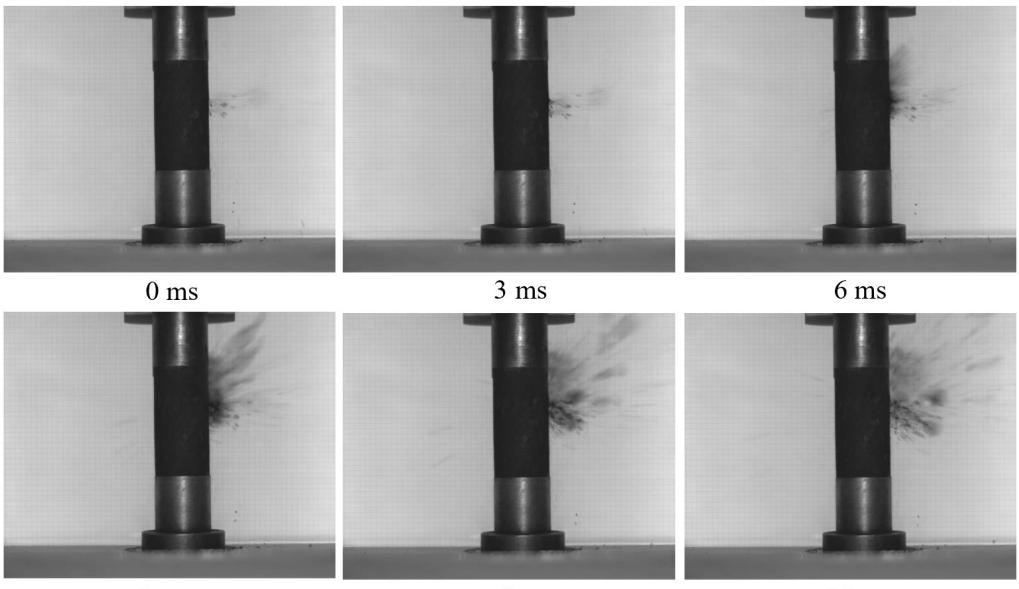

(T1)

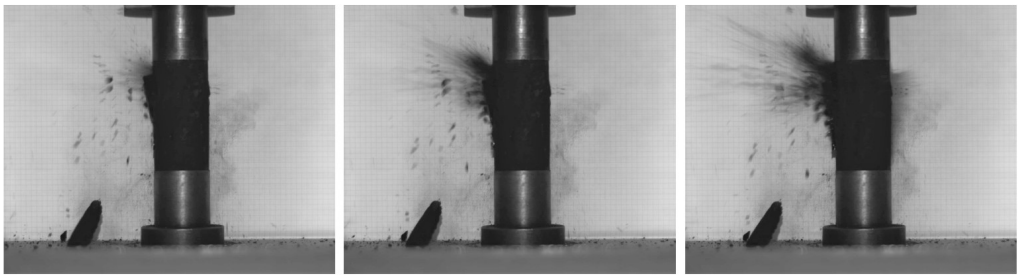

0 ms 3 ms 6 ms

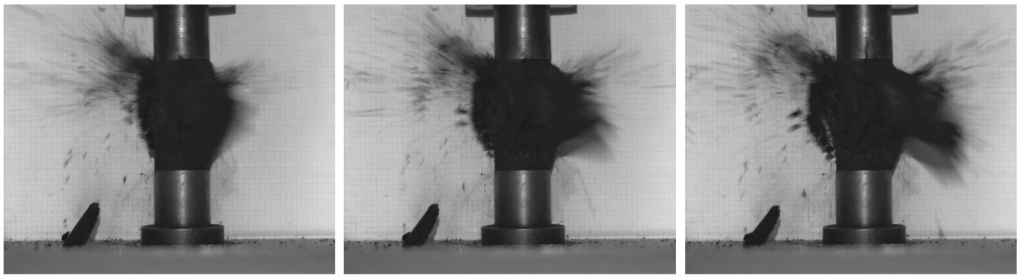

9 ms 12 ms 15 ms

(T2)

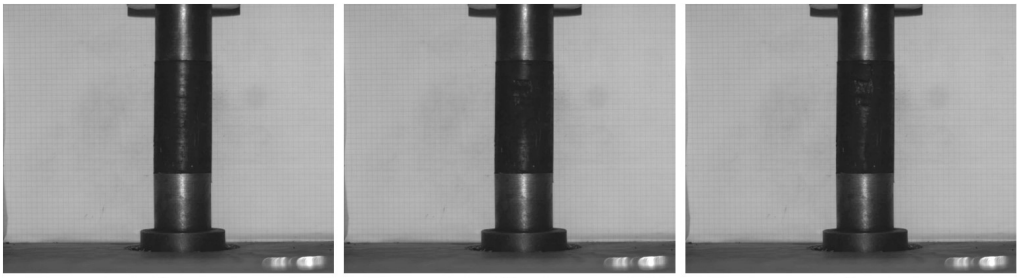

0 ms 3 ms 6 ms

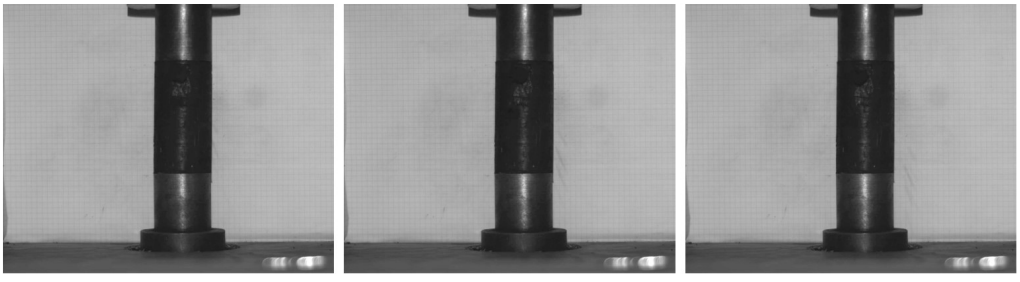

9 ms 12 ms 15 ms

(T3)

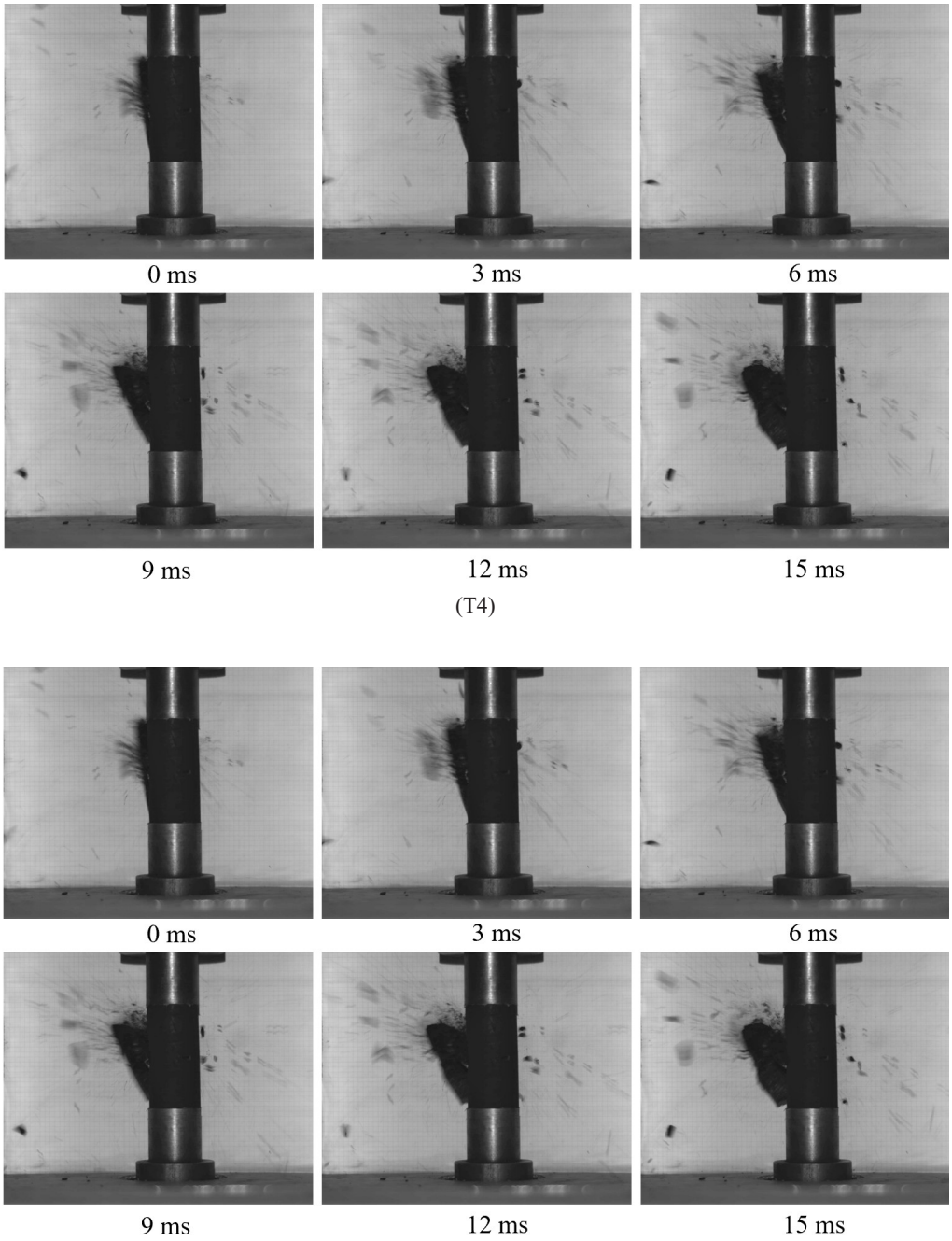

Fig. 3. Ejection or failure process

The load-deformation curves are shown in Fig. 4 (The red circle marks the moment when the particles are ejected).

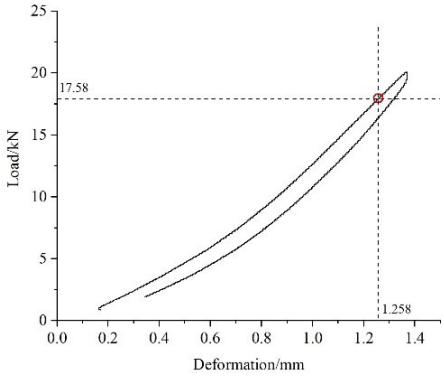

(T1)

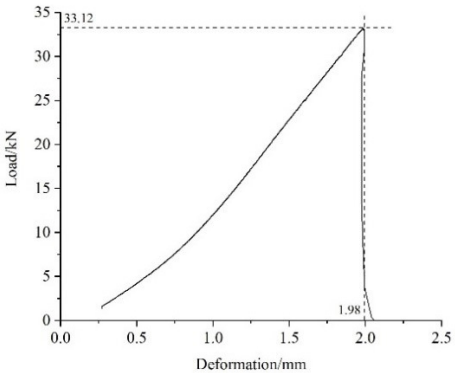

(T2)

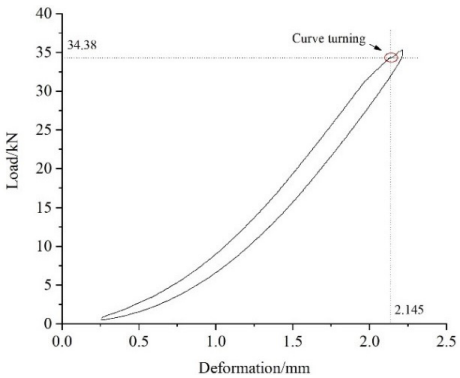

(T3)

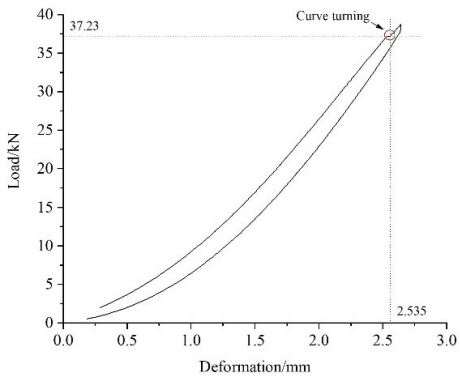

(T4)

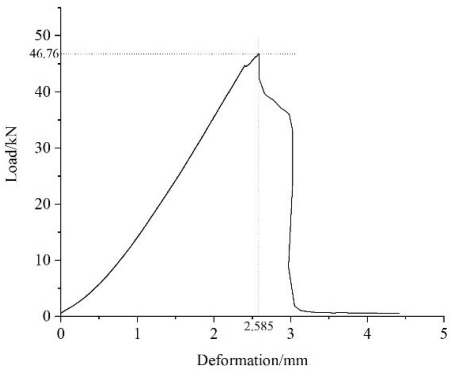

(T5)

Fig. 4. Load-Deformation curve

3.3. Discussion

The results can be divided into two groups. In T1, T3 and T4, particles ejected from the samples, whereas in T2 and T5, no ejection occurred during the loading until the samples have completely failed.

By analysing the high-speed camera images, the velocities of the ejected particles can be calculated. Fig. 5 shows the track of the particle captured by the high-speed camera in T4. The black line in the image is the distance of a particle flying during one exposure.

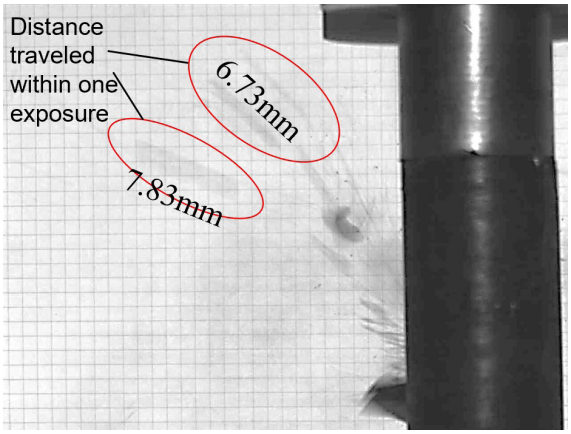

Fig. 5. Ejection of particles

By analyzing the loading and unloading curve in Fig. 4, we can obtain the values of elastic and plastic energy in T1, T3 and T4. During the loading, the testing machine works, so the area under the loading curve is the total energy absorbed by the sample. During the unloading, the elastic energy is completely released, and the plastic energy is retained as permanent deformation. Therefore, the area between the two curves is the plastic energy, as shown in Fig. 6. In T3 and

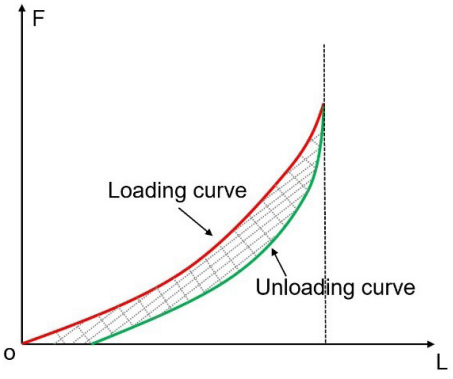

Fig. 6. Loading and unloading curve

T4, when particles are ejected from the sample, the curve turns, as highlighted in the red circle in Fig. 4. The turning of the curve causes the area of the plastic zone to increase, which means a part of the energy is lost in the form of kinetic energy.

There is no small particle ejected until the samples completely fail in T2 and T5. Fig. 7 shows the load-time curves of these two tests. The entire failure time is 38 ms and 20 ms.

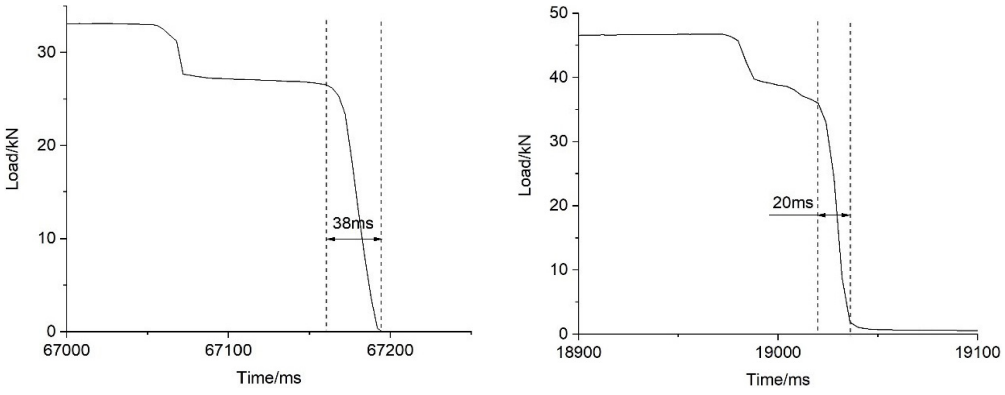

(T2) (T5)

Fig. 7. Load-time curve

The results of the experiment are shown in table 2 (Load and deformation converted to stress and strain).

TABLE 2

Experimental results

Group	Test	Density (kg/m^3)	Elastic modulus (MPa)	Average Velocity (m/s)	Stress (MPa)	Strain (10^{-2})	Elastic energy (kJ)	Plastic energy (kJ)	Energy ratio
Load then unload	T1	1211.426	2315.243	2.980	9.477	1.269	9.132	1.927	4.739
	T3	1224.464	1764.529	3.348	18.533	2.159	25.124	5.083	4.943
	T4	1222.396	1981.316	3.612	18.573	2.536	35.604	6.457	5.514
Load to failure	T2	1228.997	2218.335	3.828	17.421	1.996	—	—	—
	T5	1236.383	2086.676	3.923	25.617	2.617	—	—	—

The results are divided into two groups. The first group is the complete loading and unloading process. In the second group, there is no ejection during the loading process until complete failure. The above data shows that the velocity of the particles in the second group is greater than the in the first group. This is because the kinetic energy released is larger when the failure occurs. In the first group, there is a positive correlation between velocity and elastic energy. Fig. 8 shows the sample in T4. It can be seen that the V-shaped fracture surface formed after the ejection. The fracture surface is flat and partially attached with white patches, indicating that the fracture is extending along the weak surface.

Fig. 8. Fracture surface formed after ejection

4. Theoretical study

Assuming that the sample follows the Mohr-Coulomb criteria, the stress field can be calculated using a numerical method. Firstly, a flat model is created with 50 mm wide and 100 mm high. The parameters in T4 are used in the numerical simulation. Secondly, stress boundary conditions (18.573 MPa) are applied at the upper and lower ends, whilst the free boundary conditions are set on the left and right sides. Thirdly, radial fixed boundary conditions are applied in a small range (1mm) at the left and right sides of upper and lower ends. The boundary conditions and the maximum principal stress in the sample are as shown in Fig. 9.

It can be seen that the maximum principal stress field is X-shaped. The maximum principal stresses in the upper and lower zones are both greater than the load, and the maximum principal stresses in the left and right zones are less than the load. This shows that although the samples are all compressed, the movement trends are different. The upper and lower zones tend to be squeezed towards the middle zone, and the left and right zones tend to be squeezed out of the middle zone. These two trends ultimately result in the complete failure of the sample.

The above results are based on the assumption that the material is continuous and uniform. However, there are many cracks in the rock. Griffith [19] put forward the theory of fracture of brittle materials. The author believed that there are many uniformly and randomly distributed cracks inside the material. Under the load, the cracks tip in an unfavorable direction and can generate a large concentration of stress. So the crack starts to expand until the entire material fails.

Tensile and shear failure are the two types of crack failure, as shown in Fig. 10. Each side of the crack tip tends to move in an opposite direction. Therefore, the kinetic energy obtained by particle B should not come from A. According to the law of conservation of energy, the energy should come from the elastic energy released by particle B itself.

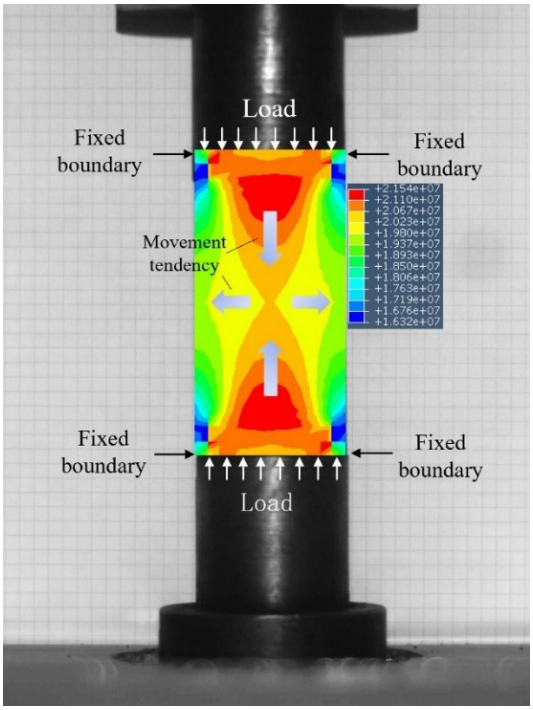

Fig. 9. Maximum principal stress

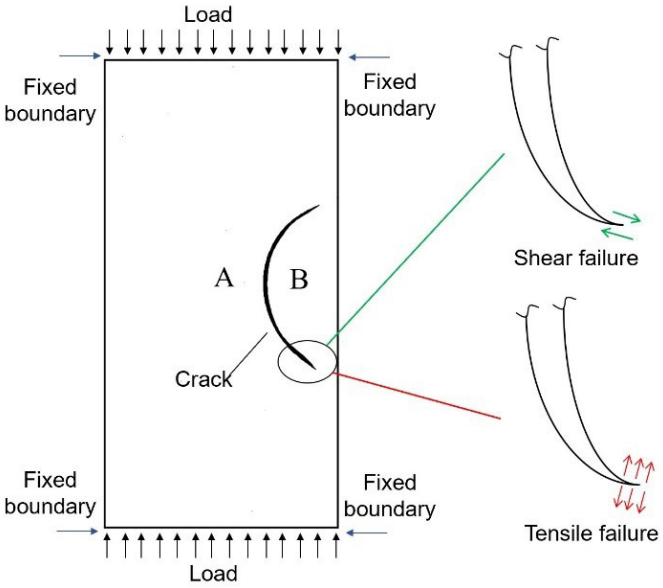

Fig. 10. Crack growth type

Based on this conclusion, the relationship between elastic and kinetic energy can be further analysed. Based on the 2D elasticity assumption, the elastic energy of B can be calculated with Eq. (1).

$$E_e = \left(\frac{\sigma^2}{2E}\right) \cdot S \tag{1}$$

where S is the area of particle B in Fig. 10, σ is the stress and E is the elastic modulus.

The kinetic energy of B can be calculated with Eq. (2).

$$E_k = \left(\frac{v^2}{2}\right) \cdot \rho \cdot S \tag{2}$$

where v is the ejection speed and ρ is the density of the sample.

From Eq. (1) and Eq. (2), we can obtain the ratio of kinetic energy to strain, represented in Eq. (3).

$$\frac{E_k}{E_e} = \frac{\rho \cdot E \cdot v^2}{\sigma^2} \tag{3}$$

The energy conversion ratios calculated with Eq. (3) are shown in table 3.

TABLE 3

Energy ratio

No.	T1	T2	T3	T4	T5
E_k/E_e	14.841%	13.164%	7.051%	9.160%	6.051%

The percentage of elastic energy converted into kinetic energy is between 6.051% and 14.841%, with an average of 10.053%. It should be noted that these results do not take into account the energy loss in plastic deformation. Otherwise, the actual percentage of elastic energy converted into kinetic energy should be smaller to a degree depending on the plastic deformation.

5. Conclusions

The process of a rock burst caused by the static load is studied experimentally and theoretically. Simulation of a rock burst is carried out using a modified uniaxial compression experiment combined with a high-speed camera system. Then the mechanism of rock burst is comprehensively discussed with numerical simulation and crack propagation mechanics.

In the simulation experiment, three of the five tests have the phenomenon that particles eject from the samples under static load. This is accompanied by a significant turning point of the load-deformation curves. This indicates that the kinetic energy is carried by the ejected particles. In the other two tests, the ejection phenomenon doesn't occur during loading. The velocity of

ejected particles is between 2 m/s and 4 m/s. The ratio of elastic energy to plastic energy is approximately 5. The duration from integrity to failure is between 20 ms and 40 ms.

By the method of numerical simulation, it can be seen that the upper and lower zones tend to squeeze toward the middle and the left and right zones tend to be squeezed outwards. Considering the point of crack growth, it is concluded that the kinetic energy of the ejected particles comes from the elastic energy released by the particles themselves. Based on this conclusion, the ratio of elastic energy to kinetic energy can be calculated, which is approximately 10%.

These conclusions can help understand the process of a rock burst under static load (such as a rock burst of mine pillar) quantitatively. Acoustic emission (AE) technology should be used in future research to obtain better results.

Acknowledgements

This work is supported by the National Natural Science Foundation of China through contracts No. 51574150, No. 51874176. Dr. Zhongxue Sun provided great help in the experiment.

References

[1] F. Ren, C. Zhu, M. He, Rock Mech. Rock Eng. **53**, 1-2(2019). DOI: 10.1007/s00603-019-01897-3

[2] G. Su Y. Shi, X. Feng, J. Jiang, J. Zhang, Q. Jiang, Rock Mech. Rock Eng. **51**, 375-389 (2018). DOI: 10.1007/s00603-017-1344-6

[3] F. Gong, Y. Luo, X. Li, X. Si, M. Tao, Tunn. Undergr. Sp. Tech. **81**, 413-427(2018). DOI: 10.1016/j.tust.2018.07.035

[4] S.H. Cho, Y. Ogata, K. Kaneko, Int. J. Rock Mech. Min. **42** (4), 561-568(2005). DOI: 10.1016/j.ijrmms.2005.01.004

[5] J. Wang, H.D. Park, Tunn. Undergr. Sp. Tech. **16** (1), 49-57(2001). DOI: 10.1016/S0886-7798(01)00030-X

[6] M.N. Bagde, V. PetorŠ, Int. J. Rock Mech. Min. Sci. **42** (2), 237-250(2005). DOI: 10.1016/j.ijrmms.2004.08.008

[7] M. Cai, H. Morioka, P.K. Kaiser, Y. Tasaka, H. Kurose, M. Minami, T. Maejima, Int. J. Rock Mech. Min. **44** (4), 538-549(2007). DOI: 10.1016/j.ijrmms.2006.09.012

[8] K. Du, M. Tao, X. Li, J. Zhou, Rock Mech. Rock Eng. **49** (9), 3437-3453(2016). DOI: 10.1007/s00603-016-0990-4

[9] R. Simon, PhD thesis, Analysis of fault-slip mechanisms in hard rock mining, McGill University, Quebec/Montreal, Canada (1999).

[10] N.G. Cook, Int. J. Rock Mech. Min. **2** (4), 389-403(1965). DOI: 10.1016/0148-9062(65)90004-5

[11] P.N. Calder, D. Madsen, Int. J. Rock Mech. Min. **26**, 3-4 (1989). DOI: 10.1016/0148-9062(89)92469-8

[12] Z.T. Bieniawski, Int. J. Rock Mech. Min. **4** (4), 407-423 (1967). DOI: 10.1016/0148-9062(67)90031-9

[13] S.P. Singh, Rock Mech. Rock Eng. **21** (2), 149-155 (1988). DOI: 10.1007/BF01043119

[14] A. Kidybiński, Int. J. Rock Mech. Min. Sci. **18** (4), 295-304 (1981). DOI: 10.1016/0148-9062(81)91194-3

[15] A. Tajduś, M. Cala, K. Tajduś, Arch. Min. Sci. **63** (3), 747-765 (2018). DOI: 10.24425/123695

[16] W.D. Ortlepp, T.R. Stacey, Tunn. Undergr. Sp. Tech. **9** (1), 59-65 (1994). DOI: 10.1016/0886-7798(94)90010-8

[17] H. Marcak, Arch. Min. Sci. **57** (1), 229-250 (2012). DOI: 10.2478/v10267-012-0016-3

[18] T.J. Williams, C.J. Wideman, D.F. Scott, Pure Appl. Geophys. **139**, 627-637 (1992). DOI: 10.1007/BF00879955

[19] A.A. Griffith, Phil. Trans. Math. Phys. Eng. Sci. **221** (582-593), 163-198 (1921). DOI: 10.1098/rsta.1921.0006